

Chapter 6

Lateral Confinement and Reduced T_N in Holmium

A well-known consequence of a strongly reduced sample size is a reduction of the ordering temperature, which was the subject of intense research on many FM materials. Farle et al. studied the thickness dependence of the ordering temperature of FM Gd films down to only a few monolayers [40]. The observed decrease of the ordering temperature with decreasing film thickness was found to be in excellent agreement with theoretical considerations that predict a scaling behavior according to Eq. 1.14. The same behavior was found in $3d$ -ferromagnets and simple antiferromagnets, like CoO. In contrast, experiments on long-period AFM structures revealed a much higher sensitivity on a reduction of the spatial dimension. An experiment performed by Ott et al. [54] on AFM holmium metal films revealed that a reduced sample dimension along the direction of the AFM modulation results in a much faster decrease of the ordering temperature than for Gd. This thickness-dependent T_N is described by Eq. 1.16 discussed in chapter 1.3.1, which includes an offset thickness d_0 [46]. While experiments on the thickness dependence in thin films are numerous, quantitative studies of the influence of lateral confinement are rare. This chapter presents experiments on holmium films that study the influence of a strong lateral confinement on the holmium ordering temperature.

In this chapter, we will first focus on the magnetic and structural properties of high-quality single-crystalline thin and ultra-thin Ho metal films grown in-situ on W(110), in order to compare with the Y/Ho/Y structures of the previous study [54]. Subsequent preparation of polycrystalline films will then allow to study the influence of lateral confinement.

6.1 Single-Crystalline Holmium Films

Single-crystalline Ho films were prepared by vapor deposition of high-purity Ho metal onto a previously cleaned W(110) single crystal using the evaporation source described in chapter 5.1. The diffraction setup allows a characterization of the sample quality during the growth process: Figure 6.1 (left panel) shows the specularly reflected intensity at a fixed scattering vector, recorded at $h\nu = 1351$ eV during deposition of Ho onto W(110) at 300 K. Due to the interference of the x rays reflected from the substrate and the growing overlayers, oscillations in the intensity occur with a period that depends on the scattering vector [132]. Hence, these growth oscillations directly monitor the number of deposited layers, which permits a precise control of the final film thickness. One oscillation represents about 17.5 \AA of added material, while the damping results from the decreasing interface contribution due to absorption of scattered photons in the holmium layers at resonance. Film preparation with the

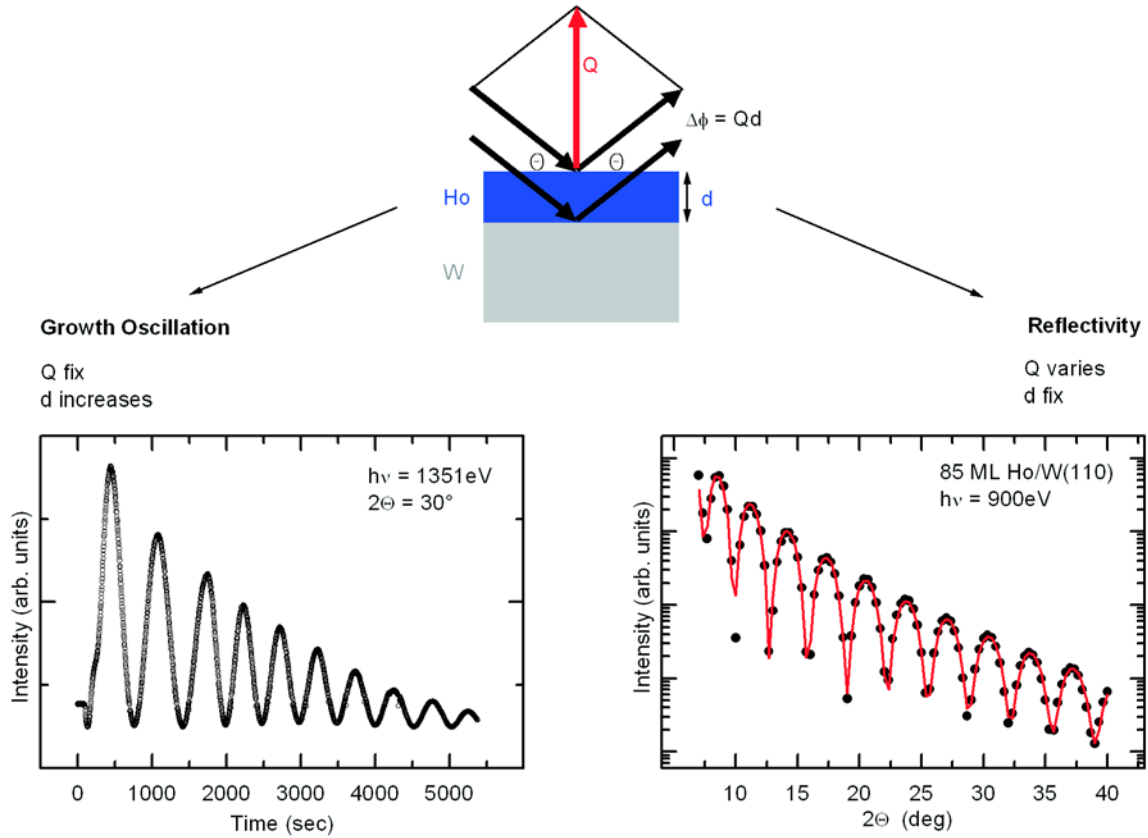


Figure 6.1: Growth and structural characterization of an 85-ML-thick Ho film. Top: Scheme of the experiment. The two waves reflected from the Ho surface and Ho/W interface are characterized by a phase shift $\Delta\phi$ given by the scattering vector Q and the sample thickness d . Left: Intensity oscillations at fixed Q at $h\nu = 1351$ eV measured during growth. Right: Non-resonant specular reflectivity from this Ho film. The red line shows a fit according to the model discussed in the text.

substrate held at 300 K results in an extended layer-by-layer growth, as evidenced by the pronounced oscillations observable up to more than 15 nm thickness. The reflectivity curve from the final film, measured at $h\nu = 900$ eV, is shown in the right panel of Fig. 6.1. The pronounced Kiessig fringes indicate a small surface and interface roughness. Indeed, a description of these data as outlined in chapter 3.2 yields a roughness of less than one monolayer. The optical parameters at 900 eV are taken from Ref. [99]. Along with the observed rocking width of the magnetic reflection of about 0.7° , these results show that films of the extremely reactive lanthanide metals can be grown with high quality in the new setup. The typical base pressure of about $1 \cdot 10^{-10}$ mbar in the present setup allows for magnetic scattering experiments for several hours.

Below the bulk ordering temperature of about 132 K, Ho metal exhibits a long period AFM structure. This incommensurate but nearly perfectly sinusoidal modulation normal to the sample surface gives rise to magnetic superstructure reflections around each chemical Bragg peak along the direction of the AFM modulation ([0001] direction) (Fig. 6.2). The distance between the magnetic and chemical reflections, τ , is given by the inverse of the helix period. In the case of the present Ho(0001) films on W(110), the [0001] direction coincides with the surface reflectivity as depicted in Fig. 6.2(c). The first chemical reflection along this direction, the (0002) Bragg peak, is not accessible in the soft x-ray

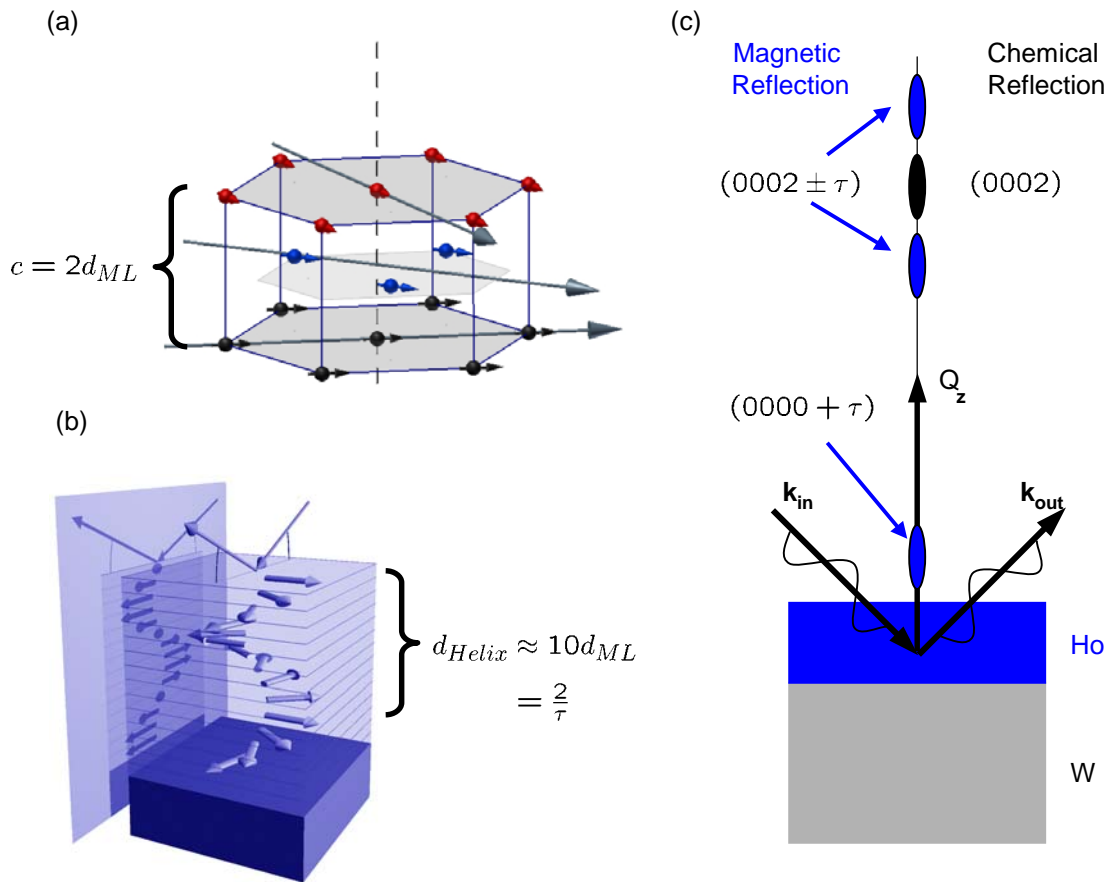


Figure 6.2: Crystal and magnetic structure of Ho. (a) The chemical hexagonal unit cell of Ho metal, including the spin direction in the AFM phase. Different colors represent different spin directions. (b) AFM helix of 10-ML period length along the [0001] direction. (c) Reciprocal space picture for the studied Ho(0001) films on W(110). The magnetic superstructure gives rise to magnetic reflections along the [0001] direction around each chemical Bragg peak at a distance τ .

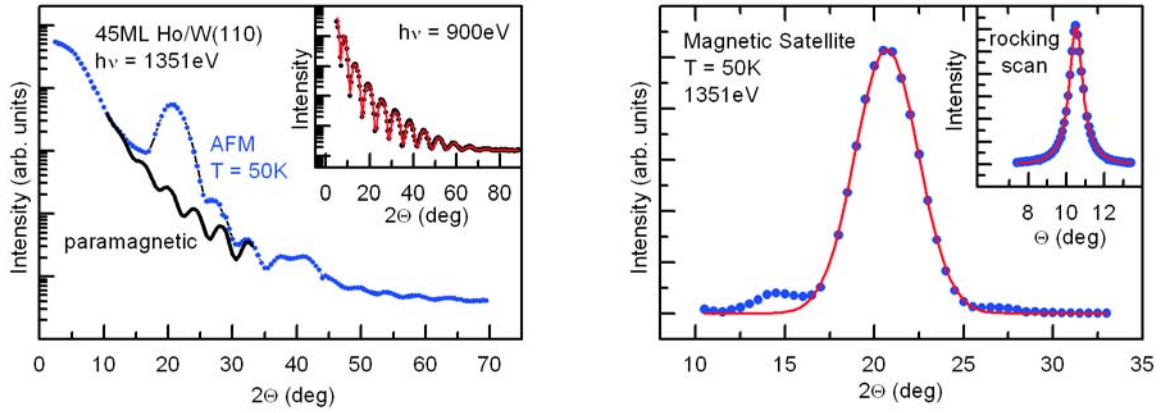


Figure 6.3: Magnetic signals at resonance of a 45-ML-thick single-crystalline Ho film. Left: Longitudinal scans at the Ho- M_5 resonance above (black) and below (blue) the ordering temperature. The inset shows the non-resonant reflectivity at 900 eV. Right: The difference of the high- and low-temperature reflectivities from the left panel. The position and width of the magnetic Bragg peak are determined from a Gaussian fit (red line). The narrow rocking curve (inset) measured at the maximum of the magnetic peak reveals the large in-plane coherence of the magnetic structure.

range. However, the first magnetic superstructure reflection ($0000+\tau$) occurs at an angle of incidence of about 10° at the Ho- M_5 absorption threshold. This resonance is accompanied by a huge enhancement of the magnetic scattering strength as evident from the intense magnetic scattering signal from a 45-ML-thick holmium film shown in Fig. 6.3. The blue curve displays the scattering signal at resonance obtained at low temperatures, while the black curve shows the persisting charge reflectivity above the ordering temperature. Unlike the non-resonant magnetic scattering case, the magnetic superstructure peak is the dominating feature at the Ho- M_5 threshold. The right panel of Fig. 6.3 depicts the magnetic signal after subtraction of the charge background. It is described by the Laue function as expected from the finite film thickness. The number of layers contributing to the magnetic signal can be determined from the peak width to (45 ± 1) ML, which perfectly agrees with the chemical thickness of the film of (46 ± 1) ML determined from the reflectivity curve at 900 eV (inset in the left panel of Fig. 6.3). Along with the small rocking width (inset in the right panel), the high quality of the magnetic structure of these in-situ prepared samples is proven.

The huge resonant enhancement of the magnetic scattering cross section, visualized in the right panel of Fig. 6.4, is accompanied by a strong and non-negligible change of the index of refraction $n = 1 - \delta + i\beta$. This is reflected in the low-angle reflectivities measured in the paramagnetic phase (left panel of Fig. 6.4). With decreasing distance to the resonance maximum at 1350 eV, the Kiessig fringes shift substantially. Directly at the resonance maximum, the Kiessig fringes are strongly suppressed as a consequence of the decreasing contribution from the W/Ho interface due to the large photon absorption in the Ho layers. Therefore, at resonance, corrections for refraction and absorption effects have to be included in the quantitative analysis of the magnetic signal, particularly at small angles of incidence. While non-resonant optical parameters β and δ are well documented in the literature, they are less precisely known at resonance. However, exploiting the characteristic changes of the low-angle reflectivity curves, the optical parameters at resonance can be quantified with high accuracy: A description of the non-resonant reflectivity (as in Fig. 6.1), applying optical parameters from literature [99], yields the film thickness and interfacial roughness. With these structural properties fixed, the subsequent fit of the reflectivities close to threshold (red lines in Fig. 6.4), yields the

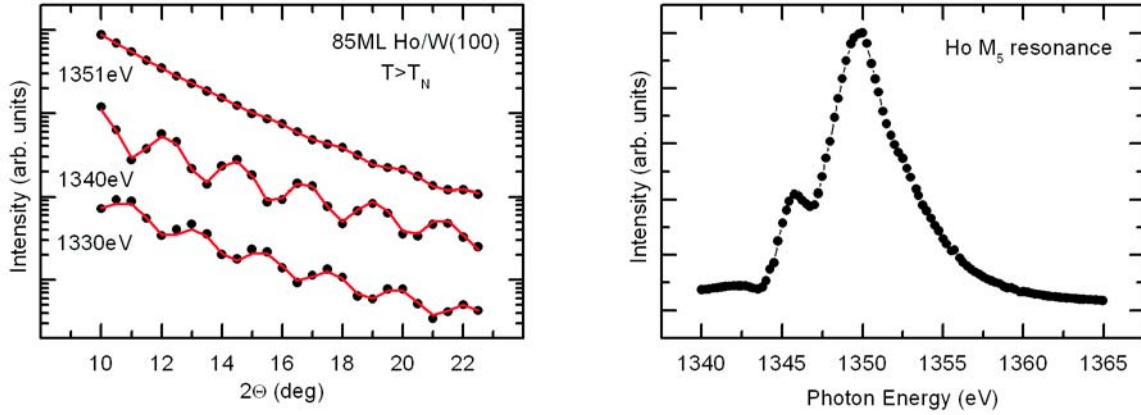


Figure 6.4: *The Ho- M_5 absorption threshold. Right: Energy-dependent intensity of the magnetic superstructure peak from a 45-ML-thick Ho film. Left: Low-angle reflectivities at photon energies close to the Ho resonance. The data are vertically shifted for clarity.*

optical parameters δ and β at resonance.

From the intense magnetic superstructure peak from only 45 ML, it is evident that the method can be applied to samples of much smaller thickness and probably even polycrystalline material. While a reduction of the sample thickness permits to study the dependence of the ordering temperature on a spatial limitation along the AFM modulation, polycrystalline growth will allow to study the influence of a lateral confinement.

Before turning to the influence of such in-plane restrictions, we shall first ensure that the prepared single-crystalline films reproduce a behavior of T_N according to Eq. 1.16. For that purpose, films of only 12 ML and 16 ML of thickness were prepared. The corresponding non-resonant low-angle reflectivity curves, shown in the left panel of Fig. 6.5, are characterized by very broad Kiessig fringes as a consequence of the small film thickness. Fits to these data yield the stated thicknesses with surface roughnesses of about one monolayer. The finite film thickness also leads to a broadening of the magnetic signal, as depicted in the center panel of Fig. 6.5. Consequently, the magnetic signal is less pronounced than in the case of the 45-ML-thick film. However, the ordering temperatures of the samples can still be determined from the temperature dependence of the magnetic scattering signal. Although the integrated magnetic intensity represents the AFM order parameter, it is sufficient to monitor the magnetic peak intensity, because neither the longitudinal nor the transversal width of the magnetic signal depend on temperature in the present case. This quantity can be easily recorded by a temperature-dependent scan at the position of the peak maximum Q_{AFM} close to the ordering temperature, as shown in the right panel of Fig. 6.5. The obtained temperature dependences of the magnetic peak intensities of the two thin films clearly reveal reduced ordering temperatures compared to an 85-ML-thick film. Close to T_N , not only the long-range ordered structure, but also magnetic short-range correlations contribute to the measured intensity, and consequently the magnetically scattered intensity does not vanish at T_N (cf. Fig. 1.4). For this reason, T_N is determined by power-law fits of the intensity, ignoring the temperature range very close to T_N . Hence, a precise quantification of the critical exponent, which can be also a thickness-dependent property, is not possible. Therefore, fits to different values of β , ranging from the three-dimensional Ising value of $\beta = 0.325$ to the mean field value of $\beta = 0.5$, were performed. The resulting T_N is only weakly sensitive to the choice of β and the variations are included in the error bars. The obtained thickness-dependent ordering tem-

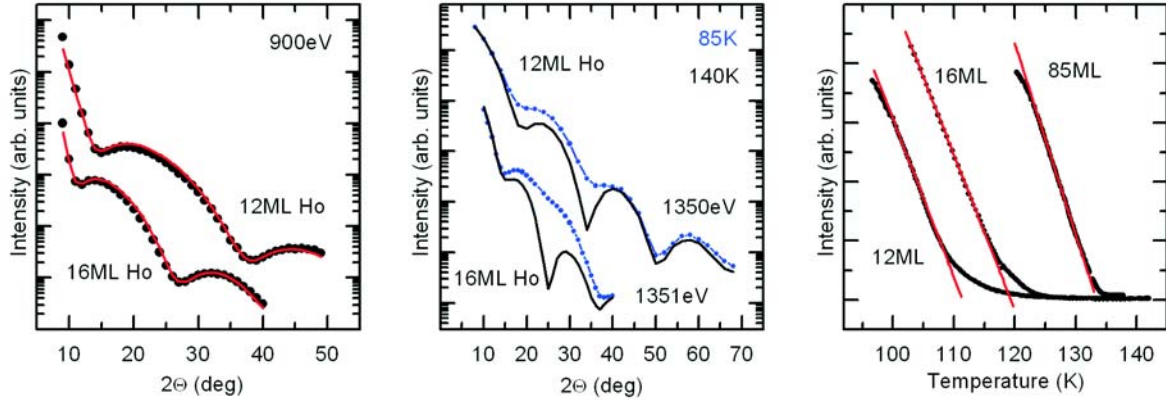


Figure 6.5: Soft x-ray scattering from ultra-thin single-crystalline Ho(0001) films. Left: Non-resonant reflectivities measured at a photon energy of 900 eV. The data are vertically shifted for clarity. Center: Corresponding magnetic scattering signals at resonance (blue). The black lines represent the persisting charge reflectivity above the ordering temperature. The data are vertically shifted for clarity. Right: Temperature-dependent intensity measured at the position of maximum magnetic contrast of the 12-ML, 16-ML and a thick single-crystalline Ho film. They are arbitrarily scaled for better comparison. The red lines represent power-law fits with the mean field critical exponent $\beta = 0.5$ (see text).

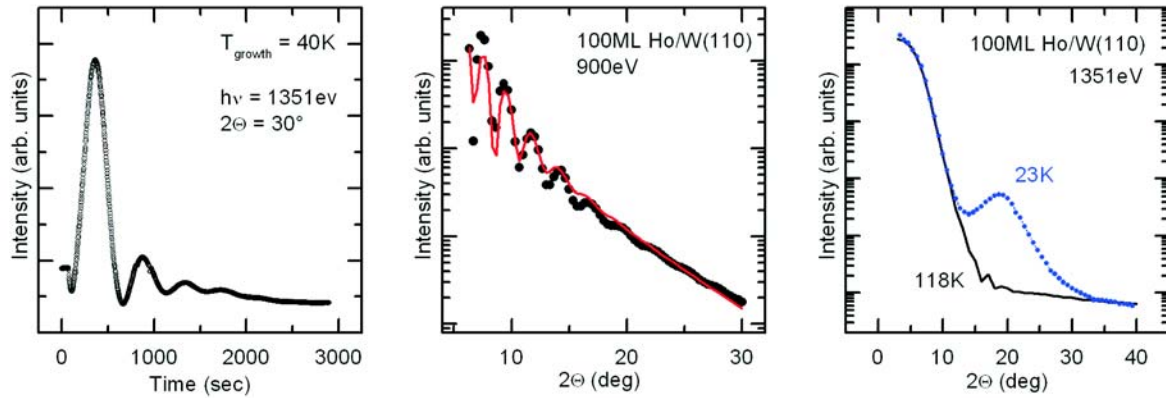


Figure 6.6: Soft x-ray scattering from a thick Ho film (100 ML) prepared at a substrate temperature of 40 K. Left: Growth oscillations. Center: Low-angle reflectivity measured at an off-resonance energy. The red line represents a fit to the data. Right: Longitudinal scans at resonance, well below the ordering temperature (blue) and at 118 K (black).

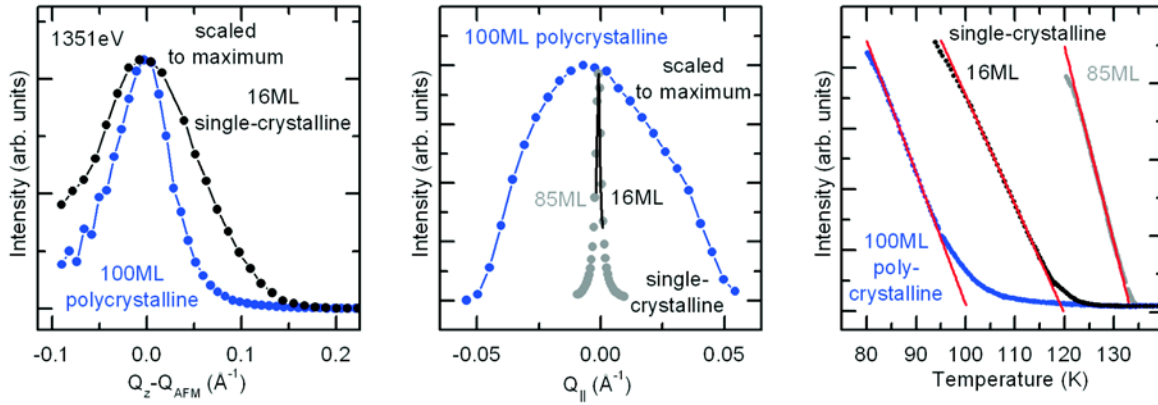


Figure 6.7: Comparison of data obtained from a 100-ML-thick polycrystalline Ho film (blue) and a single-crystalline 16-ML film. Left: Longitudinal scans at low temperatures taken at resonance. Center: Transversal intensity distribution at the position of the maximum of magnetic intensity. A rocking scan from a 85-ML-thick film, prepared at 300 K, is shown for comparison (gray). Right: Temperature-dependent intensity at the position of the magnetic peak. The curves are arbitrarily scaled for better comparison.

peratures discussed later in connection with Fig. 6.10, are in perfect agreement with the findings of the earlier study on thin holmium films on W(110) and Ho layers embedded between yttrium. This excellent agreement confirms the reported unusual fast decrease of T_N in helical antiferromagnets. Obviously, this behavior is not an exclusive property of the Y/Ho/Y system, but a general effect in thin single-crystalline Ho(0001) films, independent of details of the interface.

6.2 Polycrystalline Holmium Films

The results discussed so far show that the new UHV-diffractometer can produce high-quality single-crystalline films of the highly reactive lanthanide metal holmium. While growth with the substrate held at room temperature results in films with high in- and out-of-plane crystallinity, film preparation at a substrate temperature of 40 K is characterized by strongly damped growth oscillations as displayed in Fig. 6.6. This damping indicates a substantial increase of the surface roughness during the growth, which is also found in the strongly damped Kiessig fringes of the non-resonant reflectivity curve in Fig. 6.6. An analysis yields a total film thickness of about 100 ML and a mean surface roughness of about 7 ML. However, the fit (red line) gives only a moderately satisfactory description of the data, indicating a rather inhomogeneous macroscopic thickness and/or roughness of the sample. But even from this film, a pronounced magnetic signal is observed at low temperatures as shown in the right panel of Fig. 6.6. While the magnitude of the magnetic peak is reduced by a factor of about 20 with respect to comparable single-crystalline films, the strongly suppressed charge reflectivity renders the magnetic reflection still the dominating feature. The magnetic reflection occurs exactly at the same angle as in the case of thick single-crystalline films, which clearly demonstrates that such cold-made films exhibit AFM order with the bulk helix period. As can be seen from the black curve in the right panel of Fig. 6.6, the magnetic signal of this film has already vanished at 118 K, i.e. below the ordering temperature of the thin single-crystalline 16-ML film, clearly demonstrating the effect of lateral confinement in the polycrystalline sample.

Fig. 6.7 provides a comparison of the magnetic scattering signals from these two films. From the longitudinal peak widths displayed in the left panel, it is evident that the reduced T_N of the

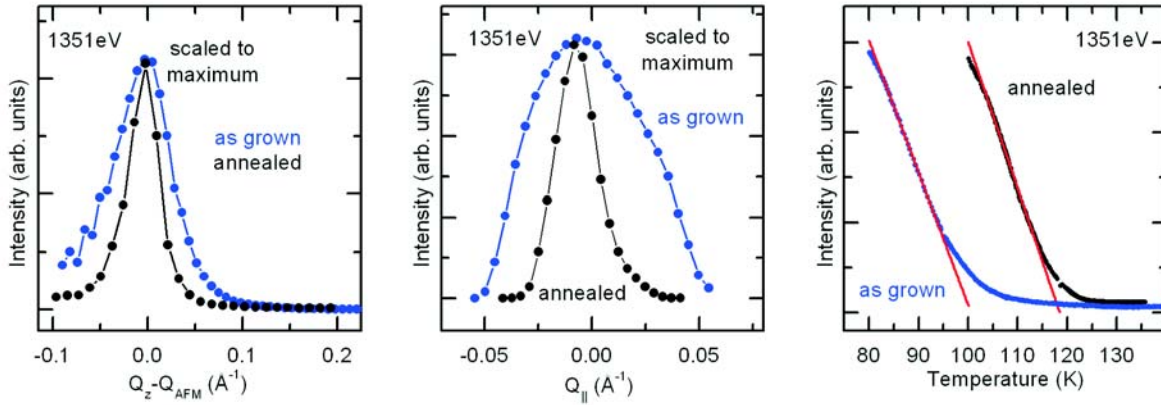


Figure 6.8: Effect of thermal treatment on polycrystalline films. Longitudinal (left) and transversal (center) magnetic intensity distribution before (blue) and after (black) annealing to 100 °C. Right: Temperature dependences of the magnetic signals. They are arbitrarily scaled for better comparison.

100 ML-thick film cannot be attributed to the strongly reduced longitudinal coherence. The peak width of the cold-made film corresponds to about 30 ML, which clearly shows that the longitudinal magnetic coherence length in such a cold-made sample does not equal the chemical thickness. Instead, the film obviously consists of smaller coherent magnetic volumes. However, the extension of these volumes along the c direction is well above the thickness regime where a reduction of the ordering temperature is expected. While both, the thin and the thick single-crystalline film are characterized by very narrow rocking curves (Fig. 6.7, center), the magnetic intensity in the case of the cold-made film is smeared out over the entire accessible in-plane reciprocal space, which suggests a very small in-plane magnetic coherence, as expected for polycrystalline samples. This finding of polycrystalline growth at low temperatures is in perfect agreement with PES¹ and LEED studies on lanthanide films [127]. The temperature-dependent intensity of the magnetic peak maximum, shown in Fig. 6.7, yields a much smaller T_N than observed for a thick single-crystalline film and even well below the ordering temperature of the 16-ML single-crystalline sample.

Moderate annealing of the cold-made film to 100°C yields only a negligible improvement of the surface roughness. However, the magnetic transversal intensity distribution sharpens significantly and also the magnetic longitudinal width decreases as shown in Fig. 6.8. Obviously, the thermal treatment increases the size of the coherent magnetic volumes in the film. This change is accompanied by an increase of T_N to about 118 K, as can be seen in the right panel of Fig. 6.8, which is still well below the ordering temperature of single-crystalline thick holmium samples. This establishes a direct relation between the size of the magnetic coherence volume and the ordering temperature. Since the reduced ordering temperature cannot be attributed to a limited longitudinal magnetic coherence, the strikingly different transversal intensity distribution identifies the responsible mechanism: a significantly reduced in-plane coherence. This conclusion is further supported by the temperature-dependent helix length. While the thin single-crystalline films are characterized by a larger helix period, i.e. a smaller value of τ as shown for the 16-ML-thin film in Fig. 6.9, all cold-made samples exactly reproduce the characteristic bulk values. Therefore, one can assume that the broad transversal intensity distribution does not only represent an angular distribution of individual crystallites but belongs to an extremely small in-plane coherence of the magnetic structure. A quantification of the lateral confinement, in particular for the system with the largest decrease of T_N , is difficult, since the measured transver-

¹Photoelectron spectroscopy.

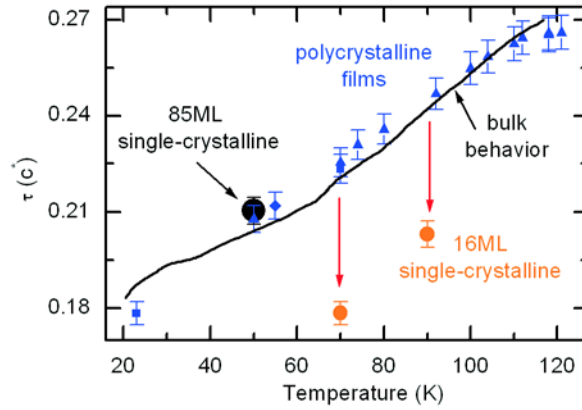


Figure 6.9: Magnetic modulation vector τ as a function of temperature. The blue symbols refer to various cold-made thick films. Black dot: in-situ prepared 85-ML-thick single-crystalline film. Black line: Holmium single crystal (from Ref. [133]). Ultra-thin single-crystalline films are characterized by a reduced τ (orange dots).

sal intensity distribution is limited by the sample horizon and displays only a fraction of the entire signal. Thus, a precise line shape analysis can be performed only to some extent. The transversal magnetic intensity distributions are analyzed by fitting Lorentzian lines to the data. According to Lee et al. [134], such a shape is expected from a distribution of domains at the surface. The half width at half maximum (HWHM) of this Lorentzian equals the inverse of the average domain size.

The final overview of the influence of lateral and longitudinal spatial confinement is given in Fig. 6.10. The decrease of the film thickness in the case of the single-crystalline films leads to a broadening of the measured longitudinal magnetic intensity distribution (Fig. 6.10(a)), while the transversal shape remains narrow. This finite film thickness causes a reduced ordering temperature (orange dots of Fig. 6.10(b)), which is well described by Eq. 1.16, in excellent agreement with an earlier study (smaller dots) [54]. In contrast, the polycrystalline films show a reduced T_N that does not depend on the longitudinal coherence length, but on the transversal width of the magnetic scattering contribution shown in Fig. 6.10(c). This experimental dependence of the ordering temperature from the in-plane width can be described by a simple mean-field model of a cubic coherent magnetic volume characterized by reduced dimensions in both in-plane directions. Assuming that the number of neighboring spins at the surface of the cube is reduced to half of the bulk number, the reduction of T_N is given according to the usual mean-field argument by the ratio of the number of surface and bulk spins:

$$T_N(n) = T_N(\infty) \left(1 - \frac{2}{n}\right), \quad (6.1)$$

where n is the inverse transversal width in units of the holmium nn spacing (3.58 \AA [135]). Equation 6.1 yields a nice description of the experimental data as depicted in Fig. 6.10(d) (red line).

In summary, high-quality single-crystalline Ho metal films were prepared in-situ. The ordering temperatures of these films, obtained from resonant magnetic scattering experiments, reveal a modified thickness dependence of T_N with respect to the behavior of short-period magnetic structures. In this way, the results of an earlier study on Y/Ho/Y sandwich structures are fully confirmed. This finding is attributed to a spatial limitation along the direction of the long-period AFM modulation. In addition, even thicker but polycrystalline films, characterized by a bulk-like magnetic structure, show a reduced ordering temperature. The bulk-like magnetic structure along the c axis and the large

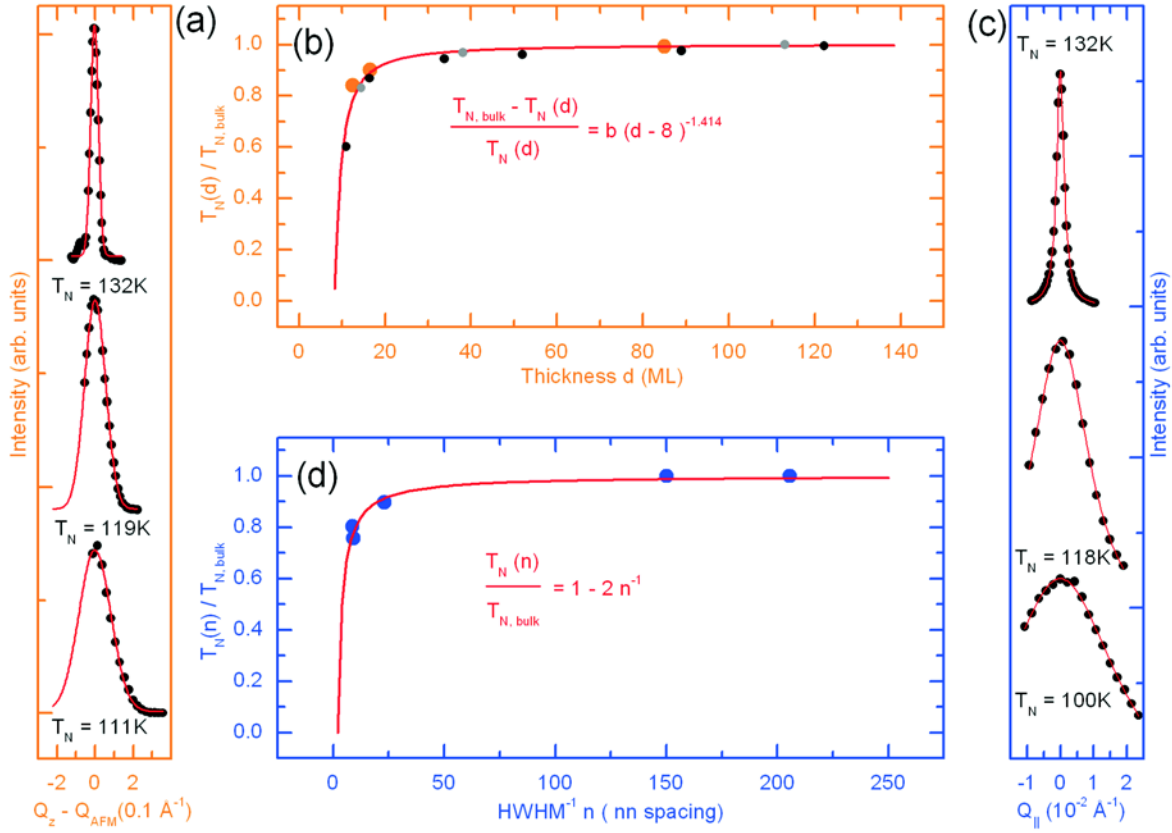


Figure 6.10: Dependence of the ordering temperature on the size of the coherent magnetic structure. (a): Longitudinal broadening of the AFM reflection as a consequence of finite film thickness. (b) Corresponding decrease of T_N with film thickness as obtained in the present study (orange dots) and from an earlier experiment on Ho films on W(110) (gray dots) and Y/Ho/Y sandwich structures (black dots). The decrease of T_N is described by Eq. 1.16 (red line), which includes an offset thickness of the order of the bulk helix period. (c): Transversal broadening of the AFM reflection in polycrystalline films. (d): Dependence of T_N on the inverse HWHM of the rocking scans shown in (c) in units of the nn distance (3.58 \AA). It is readily described by a mean-field behavior as discussed in the text.

in-plane width of the corresponding reflections clearly prove that the lateral confinement is the responsible mechanism. The size dependence of T_N is readily described by the mean-field formula Eq. 6.1, which indicates that the behavior according to Eq. 1.16 is exclusively associated with a spatial limitation along the direction of the AFM modulation.

The observed pronounced magnetic signal from only 12 ML of single-crystalline holmium as well as from the polycrystalline films clearly demonstrate the potential of resonant magnetic scattering at the lanthanide- M_5 absorption thresholds. Therefore, it should be possible to apply this method to systems characterized by much smaller coherent volumes, like nanodots, single layers or powder samples. In particular, studies of magnetic short-range correlations above the ordering temperature should be feasible for films down to very few layers. However, in the present study the AFM structure vanishes for Ho thicknesses below 10 ML, thus limiting the experimentally accessible thickness range. The following chapter presents an experiment which overcomes these restrictions.